Facile synthesis of C_{60}-nano materials and their application in High-Performance Water Splitting Electrocatalysis

Olivia Fernandez-Delgado,[a†] *Alain Rafael Puente Santiago,* [a†]* *Manuel Cano,*[b] *Juan J. Giner-Casares,* [b] *Alejandro J. Metta-Magaña,* [a] *and Luis Echegoyen.**[a]

[a] Department of Chemistry and Biochemistry, University of Texas at El Paso, 500 West University Avenue, El Paso, Texas 79968, United States

[b]Departamento de Química Física y Termodinámica Aplicada, Instituto Universitario de Nanoquímica (IUNAN), Facultad de Ciencias, Universidad de Córdoba, Campus de Rabanales, Ed. Marie Curie, E-14071 Córdoba, Spain

† These authors contributed equally.

KEYWORDS: C_{60}, nanotubes, nanosheets, surface, catalysis, HER, ORR

Abstract

Here, we report the synthesis and characterization of crystalline C_{60} nanomaterials and their applications as bifunctional water splitting catalysts. The shapes of the resulting materials were nicely tuned via a solvent engineering approach to form rhombic-shaped nanosheets and nanotubes with hexagonal close packed-crystal structures. The as-synthesized materials exhibited suitable properties as bifunctional catalysts for HER and ORR reactions surpassing by far the electrocatalytic activity of commercially available amorphous C_{60}. The C_{60} nanotubes displayed the most efficient catalytic performance rendering a small onset potential of -0.13 V vs RHE and ultrahigh electrochemical stability properties towards the generation of molecular hydrogen. Additionally, the rotating-disk electrode measurements revealed that the oxygen reduction mechanism at the nanotubes electrochemical surfaces is following an effective four-electron pathway. The improved catalytic activity was attributed to the enhanced local electric fields at the high-curvature surfaces.

Introduction

One of the most known and used allotropes of carbon is C_{60}. Since its discovery, it has attracted the attention of the scientific community and many efforts have been done to improve its properties and solubility by exohedral functionalization. [1-14] To date, fullerenes and their derivatives have been used in different applications such as new materials for molecular electronic devices and sensors,[15] photovoltaic devices,[16] materials for biomedical applications such as antivirals,[17, 18] drug delivery,[19] imaging,[20] and photodynamic therapy,[21] among others.

On the other hand, several reports have been published studying the morphology of C_{60} after crystallization with solvent assisted methods and trying to obtain new 1D and 2D nanoforms that can increase its properties and have an extent application in the field of nanotechnology.[22-26] So far, their application as nanosensors[25] and transistors[24] have been published showing how versatile and applicable these nanoforms of C_{60} can be.

Moreover, Hydrogen Evolution Reaction (HER) and Oxygen Reduction Reaction (ORR) are two catalytic processes that have been studied extensively. Because of the high cost of platinum, the search for new, cheaper and more efficient catalysts is vast. In the recent years, more reports have shown how carbon-based materials can effectively catalyze those reactions at a relative lower cost. [27-38]

In this paper, we focused our attention in using a cheap and affordable way to obtain new metal-free carbon-based catalysts to use in HER and ORR. The obtention of C_{60} nanomaterials was achieved following a reported method and the resulting structures tested as catalysts resulting an improvement of the catalytic activity when compared to the commercially available C_{60}.

Results and Discussion

The synthesis of the nanomaterials was performed following a reported process based on solvent engineering.[39] A saturated solution of pure C_{60} in toluene was filtered and placed in an ice bath until the temperature reached 15º. Then, an excess of tertbutyl alcohol was slowly added and the solutions left to rest for 15 minutes. After that time, the solutions were mixed and sonicated for 5 minutes and then, left in the refrigerator for 24 hours at a constant temperature of 15º. In the case of the nanotubes, the temperature used was 18º and the samples were re-dissolved after precipitation to obtain the tubular structures.

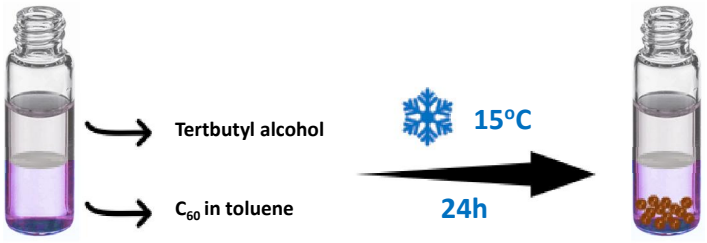

Figure 1. Schematics of the synthesis process for the C_{60} nanostructures

The nanomaterials obtained were filtered, dried and characterized by X-Ray Diffraction (XRD), Raman Spectroscopy, Scanning Electron Microscopy (SEM), Energy-dispersive X-ray spectroscopy (EDX) and Transmission Electron Microscopy (TEM).

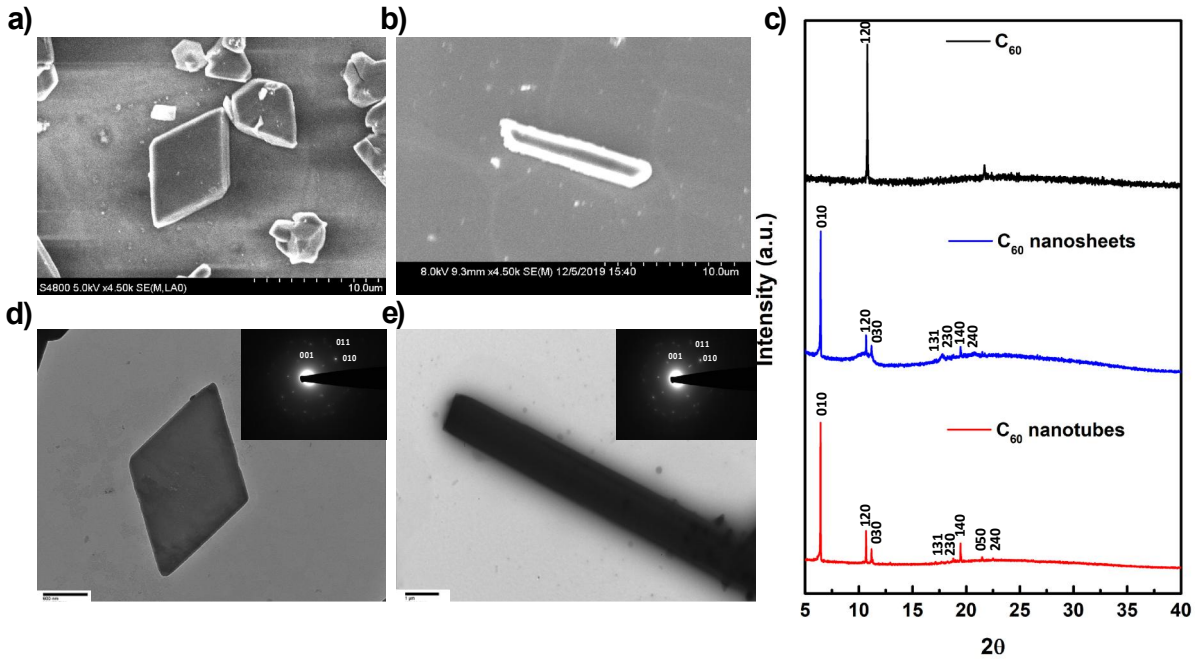

Figure 2. Characterization of the C_{60} nanostructures: SEM of a) C_{60} nanosheets and b) C_{60} nanotubes, c) XRD, and TEM of d) C_{60} nanosheets and e) C_{60} nanotubes.

SEM was performed to the nanostructures deposited onto a silicon wafer. For the C_{60} nanotubes sample, hollow tubes of around 10 µm were observed (Figure 2b). The sample was very homogeneous, and the size distribution of the nanotubes was very uniform. In the case of the C_{60}

nanosheets sample, the sheets observed were not completely uniform in terms of shape but most of them were rhombic (Figure 2a).

EDX was performed to both samples, and on the selected area on the nanotubes and nanosheets, only a carbon signal was observed (Figure S2). To investigate more about the packing at the molecular level, XRD measurements were carried out (Figure 2c). The samples were tested in thin films deposited on glass. To have a comparison, commercially available C_{60} was used as reference. In this case, the sample was found to be amorphous, having a strong signal at around 10º. For the C_{60} nanotubes and nanosheets, the XRD pattern showed a hexagonal close packing (hcp) that matches with the previous reports found in the literature.[22-24, 40]. Overall, the most important peaks of the hcp are present at around 4º, 11º, 11.5º, 17.8º, 18.5º, 19º, 21.7º and 22.6º that correspond to 010, 120, 030, 131, 230, 140, 050 and 240 facets respectively.

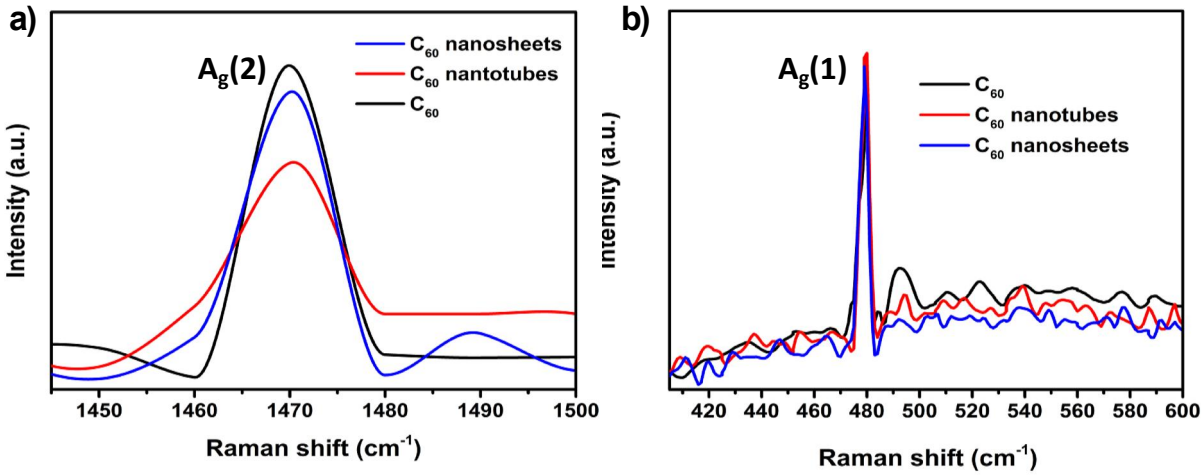

Figure 3. Raman characterization of the C_{60} nanostructures.

Raman measurements were carried out and the typical A_g (2) and A_g (1) bands at around 1470 and 480 cm^{-1} were present in all samples (Figure 3a and b). It is worth to mention that no shift was observed in any of the samples when compared to amorphous C_{60}. UV-Vis characteristics were measured, and the results showed that for samples at the same concentration there is not a pronounced difference in the absorption (Figure S1).

Electrochemical HER analysis was carefully performed for C_{60}, C_{60} nanosheets and C_{60} nanotubes samples in acidic solution (0.5 M H_2SO_4 at 2 $mV \cdot s^{-1}$), under static (Figure 4a) and dynamic (Figure 4c) conditions, to both assess their catalytic performance as cathode materials for water splitting

and explore the effect of the dimensionality of the 0D C_{60} molecules,1D C_{60} nanotubes, and 2D C_{60} nanosheets. It is worth noting that this is the first time, at the best of our knowledge, that the electrocatalytic properties of different kinds of shape-defined carbon-based materials, formed from the supramolecular interactions of fullerenes molecules, are reported. Our findings revealed that C_{60} molecules exhibited the worse HER properties with a large onset overpotential close to -0.54 V, which can be linked to the very weak interactions between the hydrogen adsorbed species and the nanocage surfaces, which exhibit a high positive value of ΔG_H=0.44 eV.[27] On the other hand, the C_{60} nanotubes showed very promising HER performances delivering a small onset overpotential of -0.13 V and a Tafel slope of 84 mV · dec^{-1}, that significantly surpassed the values of -0.21 V and 340 mV·dec^{-1} obtained for the onset overpotential and the Tafel slope of the C_{60} shaped rhombic nanosheets, respectively (Figure 4a and b).

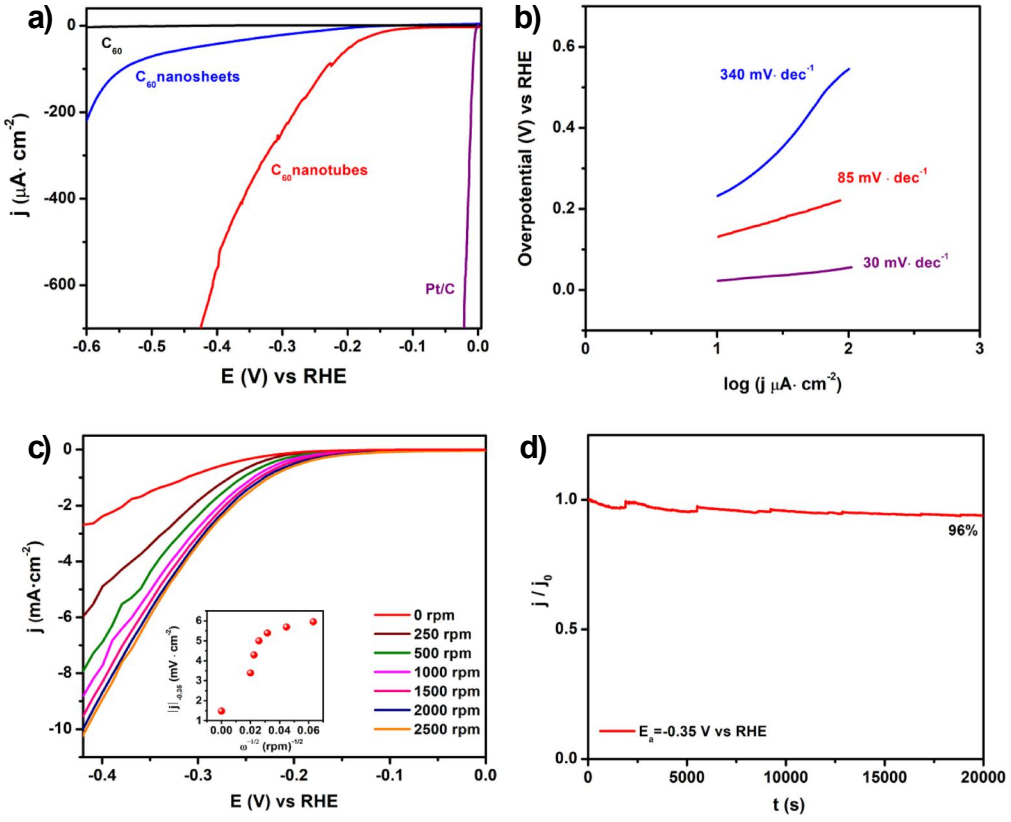

Figure 4. a) LSVs under static conditions and b) corresponding Tafel plots for HER of C_{60}, C_{60} nanosheets and C_{60} nanotubes in 0.5 M H_2SO_4 at 2 mV·s^{-1}, c) Rotating disk voltammograms (RDVs) curves at different rotation rates for the C_{60} nanotubes. Inset shows the j vs $\omega^{-1/2}$ plots, d) *I-t* curve of the C_{60} nanotubes at -0.35 V vs RHE.

These results indicate that the electrocatalytic efficiency towards the obtention of hydrogen molecules is significantly improved on the curved C_{60} nanotubes surfaces. It has been recently established that the dimensionality of metal-free carbon-based electrocatalysts can strikingly change their electrocatalytic properties through tuning the mass-transport capabilities. [28] Li Song *et. al* have shown that the mass transfer of protons processes is improved on Pt-single atoms on nanosized onion-like carbons instead of Pt-functionalized 2D graphene materials owed to the influence of very intense localized electric fields at the curved surfaces. This phenomenon, called *"tip effect"*, is able to promote the increment of reactant species at very hot active sites of the electrochemical curved interfaces, which upgrades several times the electrocatalytic activity of the curved surfaces compared with the flat materials due to the lowering of the ΔG for the hydrogen adsorption processes.[29] Similarly, the boosting of the electroreduction of CO_2 molecules at high-curvature nanostructured surfaces published by Sargent *et. al* was attributed to the action of very strong electric fields at nanoconfined spaces of the electrochemical interfaces.[30] Therefore, we propose that the electronic environment, as well as the mass transport properties, might be different for clusters of C_{60} molecules located at high-curvature areas, which could give rise to an enhanced local electric field in the aforementioned nanosurfaces and increase the hydrogen cations concentrations around the active sites, facilitating the electrocatalytic HER activity. The surface area is also another important factor that can determine the catalytic activity of carbon-based water splitting electrocatalysts.[31] Obviously, the carbon nanotubes supramolecular structures possess by far larger surface area values which contribute to increasing the number of active sites and therefore the catalytic yields.

The HER mechanistic pathway was evaluated by rotating disk electrode measurements at different rotation rates (i.e. from 250 to 2500 r.p.m.). In addition, -417 mV was the obtained overpotential at 10 $mA \cdot cm^{-2}$ at 2500 rpm, which is an essential parameter to know the efficiency of these type of HER electrocatalysts and, in turn, suggest an increment of the catalytic performances of the C_{60} nanotubes at dynamic conditions. [32, 33] Figure 4c confirmed that, for C_{60} nanotubes electrocatalysts, protons mass diffusion is the limiting stage, and therefore, the Heyrovsky step may be the rate-determining step (RDS):[34]

$$C_{60}NT\text{-}H + H_3O^+ + e^- \leftrightarrow H_2 + H_2O + C_{60}NT \qquad \text{Eq. 1}$$

The HER durability test of the best electrocatalyst (C_{60} nanotubes) was performed by chronoamperometry at a constant potential of -350 mV vs RHE, demonstrating the suitable electrochemical stability of C_{60} nanotubes (Figure 4d). To further confirm the good long-term stability, LSV curves were obtained after the durability test (Figure S4).

The electrocatalytic performances of C_{60}, C_{60} nanosheets, and C_{60} nanotubes were successfully tested toward ORR in alkaline media (Figure 5). As shown in Figure SX, under O_2-saturated conditions the three samples exhibit very well-defined ORR cathodic peaks that are not present under Ar-saturated environments, indicating that the oxygen electroreduction processes are taking place at the electrochemical interfaces. To gain further insights into the oxygen reduction reaction, LSV measurements were performed at 0.5 M NaOH, 5 $mV \cdot s^{-1}$. The onset ORR potentials were 0.68 V, 0. 73 V and 0.75 V for C_{60}, C_{60} nanosheets and C_{60} nanotubes, respectively. Noticeably, the positive shifts of the C_{60} onset potential when they form nanosheets and nanotubes are 150 mV and 170 mV, respectively, which clearly reveals that the fullerene self-assembly processes are a suitable strategy to enhance the electrocatalytic activity of the individual molecules. It is important to highlight that they are not huge differences in the catalytic behavior of C_{60} nanosheets and C_{60} nanotubes, most likely due to the ineffective action of the tip effect on the adsorption of oxygen molecules. Therefore, the improved ORR activity of fullerenes organized into nanosheets and nanotubes could be attributed to the 3D interconnected very fine porous which facilitates the diffusion of the oxygen molecules to the active sites and increase the surface area and therefore the number of ORR active sites. Figure 4b and 4d show the ORR polarization curves recorded at different rotation rates and the resulting K-L plot of the C_{60} nanotubes material, respectively. The excellent fitting demonstrates a first-order reaction toward dissolved O_2 [***10.1021/cm500805c***], [***42***]. For all the voltammograms, background currents measured under saturated Ar conditions at the same potential scan rate (5 $mV \cdot s^{-1}$) were subtracted from the respective curves to avoid the capacitive contributions. From the K-L plots and using the K-L equations, [41, 42] the average number of electrons transferred (n) per oxygen molecule at -0.1 V vs RHE was calculated (see Table 1). The number of electrons exchanged for O_2 molecules in the C_{60} nanotubes electrochemical interfaces is close to 4, suggesting that the ORR reaction is following the most efficient electron pathways mechanism.

Table 1. Onset potential values (E_{on}) and average number of electrons transferred for O_2 molecule (n_e) at -0.1 V vs RHE obtained from plots in Figure 5b and 5c, respectively.

ORR Catalyst	E_{on} (V)	n_e	J_K (mA·cm^{-2})
C_{60} nanotubes	-0.125	4.390	10.41

Finally, the chronoamperometric behavior of C_{60} nanotubes in O_2-saturated at 0.7 V vs RHE were performed to unravel its long-term stability properties. The nanotubes showed an excellent electrochemical stability at basic environments, maintaining 90 % of the initial current applied after 20000 s.

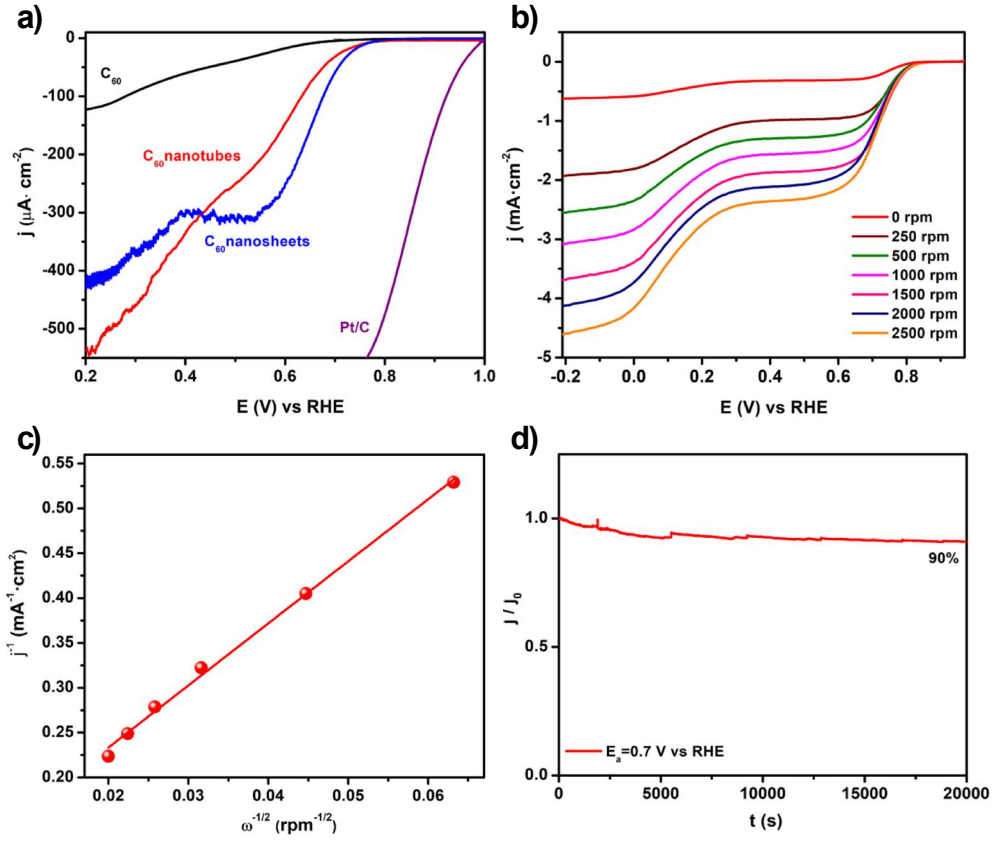

Figure 5. a) ORR polarization curves of C_{60}, C_{60} nanosheets and C_{60} nanotubes under static conditions b) RDVs at different rotation rates for the C_{60} nanotubes in 0.5 M NaOH 5 mV · s^{-1}, c)

Koutecky-Levich plots obtained from Figure 4b at -0.1 V vs RHE and d) *I vs t* curve of the C_{60} nanotubes at 0.7 V vs RHE.

Materials and methods

All chemicals were reagent grade. C_{60} was purchased 99.9% from SES Research. UV Vis was performed in a Cary Varian 5000 instrument. SEM and EDX were performed in a ZEISS Sigma field-emission scanning electron microscopy, where the electron beam was accelerated in the range of 5V to 30 kV. XRD characterization was done in Panalytical Empyrean 2 using a reflection-transmission spinner and Raman measurements were taken in a Thermo Scientific DXR SmartRaman with a 532 nm lamp. TEM was performed on a H-7650 (Hitachi High Technologies, Dallas, TX) equipped with a model XR611 mid-mount digital image camera (Advanced Microscopy Techniques, Woburn, MA).

The HER and ORR performances of the C_{60}, C_{60} nanosheets and C_{60} nanotubes were performed on an electrochemical workstation (CHI 660D) with a three-electrode system. Glassy carbon, Ag/AgCl (3M KCl) and graphite rod electrodes were used as the working, reference and counter electrode, respectively, for both HER and ORR reactions. 0.5 M H_2SO_4 and 0.1 M NaOH solutions were used as electrolytes for the HER and ORR reactions, respectively. To make the working electrode, 1 mg of the catalysts were dispersed in 1 mL of toluene and, subsequently, 10 µl of ink were deposited on the surface of the glassy carbon electrode. Linear sweep voltammetry (LSV) was carried out in 0.5 M H_2SO_4 solutions at 2 $mV \cdot s^{-1}$ and O_2-saturated 0.5 M NaOH solution at 5 $mV \cdot s^{-1}$ for HER and ORR reaction, respectively. Rotating disk electrode (RDE) measurements were performed using a glassy carbon (GC) disk (5 mm in diameter; A = 0.2 cm^2) electrode from Pine Instrument Co.

Conclusions

In this work, fullerene C_{60} has been used as building blocks to fabricate shaped-defined carbon-based electrocatalysts through a solvent engineering strategy. Through the methodology, rhombic-shaped 2D nanosheets and 1D nanotubes with hexagonal close-packed structures were successfully obtained. The as-synthesized C_{60} nanomaterials were tested as bifunctional catalysts for HER and

ORR. The obtained results showed an enhancement on the catalytic activity of the nanomaterials when compared to the commercially available amorphous C_{60}. The best performance was observed for the C_{60} nanotubes with a very small HER overpotential of -0.13 V and an excellent electrochemical stability over time, retaining 96 % of the initial applied current. In addition, these materials showed a promising behavior for ORR with an onset potential of 0.73 V and 0.75 V for C_{60} nanosheets and C_{60} nanotubes, respectively. These values represent 0.15 V and 0.17 V more than the measured value for C_{60}. For the best material, that was the C_{60} nanotubes, we performed rotating disk electrode studies and the results reveled an efficient 4-electron mechanism in ORR. The fullerene self-assembly process constituted a suitable strategy to obtain relatively cheap and efficient materials that can act as bifunctional metal-free catalysts.

Acknowledgements

The authors thank the US National Science Foundation (NSF) for generous support of this work under the NSF-PREM program (DMR 1205302), CHE-1408865 (to L.E.), and 1401188 (to F. D.). The Robert A. Welch Foundation is also gratefully acknowledged for an endowed chair to L. E. (grant AH-0033). For use of the XRD instrument, the authors thank the DoD-HBCU Program (Grant No 64705CHREP). J.J.G.-C. acknowledges the Ministry of Economy and Competitiveness (MINECO) of Spain for a "Ramon y Cajal" contract (#RyC-2014-14956), and for the MANA (CTQ201-83961-R) and JEANS (CTQ2017-92264-EXP) projects, co-financed with European Regional Development Funds (FEDER). M.C. thanks FEDER and Andalusian Government (Consejería de Economía, Conocimiento, Empresas y Universidades, Junta de Andalucía) of Spain for the financial support through UCO-1263193 project.

ASOCIATED CONTENT

Supporting Information

UV-Vis and EDX characterization for C_{60}, C_{60} nanotubes and C_{60} nanosheets. Cyclic Voltammogram under Ar-saturated solutions and Oxygen-saturated solution for C_{60}, C_{60} nanotubes and C_{60} nanosheets. LSV after durability tests for C_{60}, C_{60} nanotubes and C_{60} nanosheets.

AUTHOR INFORMATION

Corresponding Author:

***Email:** echegoyen@utep.edu

arpuentesan@utep.edu

Conflict of interest

No conflict of interest to declare

References

1. P. Choubey, A. Oudhia, and R. Dewangan, *Recent Res. Sci. Technol*, 2012, **4**, 99-101.
2. W. Kratschmer, L. D. Lamb, K. Fostiropoulos and D. R. Huffman, *Nature.*, 1990, **347**, 354-358.
3. A. Hirsch and M. Brettreich, in *Fullerenes*, Wiley-VCH Verlag GmbH & Co. KGaA: Weinheim, Germany, 2004, pp. 383-415.
4. A. Hirsch, *Angew. Chem. Int. Ed.*, 1993, **32**, 1138-1141.
5. A. Hirsch, in *Fullerenes and Related Structures*, Springer Berlin Heidelberg, 1999, vol. 199, ch. 1, pp. 1-65.
6. C. Muqing, XingLu, R. C. Maira, I. Marta and E. Luis, in *Endohedral Metallofullerenes*, CRC Press, 2014, DOI: doi:10.1201/b17840-7

10.1201/b17840-7, pp. 173-210.

7. C. Thilgen, A. Herrmann and F. Diederich, *Angew. Chem. Int. Ed.*, 1997, **36**, 2268-2280.
8. N. Martin, *Chem. Commun.*, 2006, DOI: 10.1039/b601582b, 2093-2104.
9. A. Hirsch and M. Brettreich, in *Fullerenes*, Wiley-VCH Verlag GmbH & Co. KGaA, 2005, DOI: 10.1002/3527603492.ch1, pp. 1-48.
10. H. W. Kroto, J. R. Heath, S. C. O'Brien, R. F. Curl and R. E. Smalley, *Nature.*, 1985, **318**, 162-163.

11. E. Castro, J. Murillo, O. Fernandez-Delgado and L. Echegoyen, *J. Mater. Chem. C.*, 2018, **6**, 2635-2651.
12. L.-L. Deng, S.-Y. Xie and F. Gao, *Adv. Electron. Mater.* , 2017, DOI: 10.1002/aelm.201700435, 1700435.
13. L. Pasimeni, A. Hirsch, I. Lamparth, A. Herzog, M. Maggini, M. Prato, C. Corvaja and G. Scorrano, *J. Am. Chem. Soc.*, 1997, **119**, 12896-12901.
14. P. W. Fowler, *J. Chem. Soc., Faraday Trans.*, 1995, **91**, 2241-2247.
15. C. A. Martin, D. Ding, J. K. Sorensen, T. Bjornholm, J. M. van Ruitenbeek and H. S. van der Zant, *J. Am. Chem. Soc.*, 2008, **130**, 13198-13199.
16. C.-Z. Li, H.-L. Yip and A. K. Y. Jen, *J. Mater. Chem.*, 2012, **22**, 4161-4177.
17. S. H. Friedman, D. L. DeCamp, R. P. Sijbesma, G. Srdanov, F. Wudl and G. L. Kenyon, *J. Am. Chem. Soc.*, 1993, **115**, 6506-6509.
18. E. A. Khakina, O. g. A. Kraevaya, M. L. Popova, A. S. Peregudov, S. I. Troyanov, A. V. Chernyak, V. M. Martynenko, A. V. Kulikov, D. Schols and P. A. Troshin, *Org. Biomol. Chem.*, 2016, DOI: 10.1039/c6ob02251k.
19. A. Montellano, T. Da Ros, A. Bianco and M. Prato, *Journal*, 2011, **3**, 4035-4041.
20. Z. Chen, L. Ma, Y. Liu and C. Chen, *Theranostics.*, 2012, **2**, 238-250.
21. P. Mroz, G. P. Tegos, H. Gali, T. Wharton, T. Sarna and M. R. Hamblin, *Photochem. Photobiol. Sci.*, 2007, **6**, 1139-1149.
22. M. Yao, B. M. Andersson, P. Stenmark, B. Sundqvist, B. Liu and T. Wågberg, *Carbon*, 2009, **47**, 1181-1188.
23. R. Colle, G. Grosso, A. Ronzani, M. Gazzano and V. Palermo, *Carbon*, 2012, **50**, 1332-1337.
24. C. Larsen, H. R. Barzegar, F. Nitze, T. Wågberg and L. Edman, *Nanotechnology*, 2012, **23**, 344015.
25. J. A. Rather, A. J. Al Harthi, E. A. Khudaish, A. Qurashi, A. Munam and P. Kannan, *Analytical Methods*, 2016, **8**, 5690-5700.
26. M. Sathish and K. i. Miyazawa, *J. Am. Chem. Soc.*, 2007, **129**, 13816-13817.
27. T. He, G. Gao, L. Kou, G. Will and A. Du, *J. Catal.*, 2017, **354**, 231-235.
28. L. Yang, J. Shui, L. Du, Y. Shao, J. Liu, L. Dai and Z. Hu, *Adv. Mater.*, 2019, **31**, 1804799.

29. D. Liu, X. Li, S. Chen, H. Yan, C. Wang, C. Wu, Y. A. Haleem, S. Duan, J. Lu, B. Ge, P. M. Ajayan, Y. Luo, J. Jiang and L. Song, *Nat. Energy*, 2019, **4**, 512-518.
30. M. Liu, Y. Pang, B. Zhang, P. De Luna, O. Voznyy, J. Xu, X. Zheng, C. T. Dinh, F. Fan, C. Cao, F. P. G. de Arquer, T. S. Safaei, A. Mepham, A. Klinkova, E. Kumacheva, T. Filleter, D. Sinton, S. O. Kelley and E. H. Sargent, *Nature*, 2016, **537**, 382-386.
31. L. Zhang, J. Xiao, H. Wang and M. Shao, *ACS Catalysis*, 2017, **7**, 7855-7865.
32. D. Alba-Molina, A. R. Puente Santiago, J. J. Giner-Casares, E. Rodríguez-Castellón, M. T. Martín-Romero, L. Camacho, R. Luque and M. Cano, *J Mater Chem A*, 2019, **7**, 20425-20434.
33. D. Rodríguez-Padrón, A. R. Puente-Santiago, M. Cano, A. Caballero, M. J. Muñoz-Batista and R. Luque, *ACS Appl. Mater. Interfaces*, 2020, **12**, 2207-2215.
34. C. Costentin, M. Robert and J.-M. Savéant, *Chem. Rev*, 2010, **110**, PR1-PR40.
35. X. Wang, A. Vasileff, Y. Jiao, Y. Zheng and S.-Z. Qiao, *Adv. Mater.*, 2019, **31**, 1803625.
36. R. Paul, L. Zhu, H. Chen, J. Qu and L. Dai, *Adv. Mater.*, 2019, **31**, 1806403.
37. L. Tao, Y. Wang, Y. Zou, N. Zhang, Y. Zhang, Y. Wu, Y. Wang, R. Chen and S. Wang, *Adv. Energy Mater.*, **n/a**, 1901227.
38. L. Dai, *Curr. Opin. Electrochem.*, 2017, **4**, 18-25.
39. M. Sathish, K. i. Miyazawa, J. P. Hill and K. Ariga, *J. Am. Chem. Soc.*, 2009, **131**, 6372-6373.
40. J. A. Rather, A. J. Al Harthi, E. A. Khudaish, A. Qurashi, A. Munam and P. Kannan, *Anal. Methods*, 2016, **8**, 5690-5700.
41. S. Guo, S. Zhang, L. Wu and S. Sun, *Angew. Chem*, 2012, **51**, 11770-11773.
42. A. Franco, M. Cano, J. J. Giner-Casares, E. Rodríguez-Castellón, R. Luque and A. R. Puente-Santiago, *Chem. Comm*, 2019, **55**, 4671-4674.

Table of content (TOC)